RSC Advances

ROYAL SOCIETY OF CHEMISTRY

www.rsc.org/advances

Journal Name

RSCPublishing

ARTICLE

Layer-by-Layer Assembly of Low-Temperature-Imprinted Poly(methacrylic acid)/Gold Nanoparticle Hybrids for Gaseous Formaldehyde Mass Sensing †

Naseer Iqbal,[a,b,c] Adeel Afzal*[a,b,d] and Adnan Mujahid[a,e]

Cite this: DOI: 10.1039/x0xx00000x

Received 00th January 2012,
Accepted 00th January 2012

DOI: 10.1039/x0xx00000x

www.rsc.org/

The design of gas-phase molecular recognition elements capable of detecting sub-ppm level indoor air pollutants, e.g. formaldehyde at room temperature with substantially low cross-sensitivity and fast response and recovery kinetics is a challenge. In an effort to realize such a device, low-temperature formaldehyde imprinting and layer-by-layer assembly of imprinted poly(methacrylic acid) and core-shell gold nanoparticles to fabricate imp-PMAA/Au-NPs hybrid or sandwich structures are reported. 10 MHz Quartz microbalance (QMB) coated with imp-PMAA/Au-NPs hybrid layer (optimized thickness: 100 ± 20 nm) is used as transducer. Control measurements performed at 25°C and 50% relative humidity (RH) reveal 2-9 fold increased sensor response of Imp-PMAA/Au-NPs hybrid layer toward gaseous formaldehyde (1 ppm) as compared to other tested materials. Imp-PMAA/Au-NPs hybrid sensor exhibits high selectivity toward formaldehyde due to a combination of the non-covalent dispersion interactions of formaldehyde with the molecular recognition sites and enhanced surface area. Further experiments reveal fast response and recovery times (28 and 13 sec, respectively) of imp-PMAA/Au-NPs hybrid sensor with low detection limit (152 ppb). Furthermore, excellent sensor characteristics such as complete reversibility, repeatability, and minimal humidity effect indicate that layer-by-layer assembled imp-PMAA/Au-NPs hybrid sensor is useful for potential applications in monitoring indoor air quality.

Introduction

Poor indoor air quality has a radical impact on human health that has not only increased the anxiety for healthier surroundings, but has also gained the attention of scientists to develop portable devices for continuous indoor air surveillance. Formaldehyde (H_2CO), one of the most common and toxic indoor air pollutants, is inadvertently released into the ambient atmosphere from various domestic resources involving combustion of wood, paper, cigarettes, mosquito coils, as well as high temperature frying and cooking, paints and varnishes, and photochemical oxidation of hydro-carbons.[1–4] The occupational safety and health administration (OSHA) has set the permissible exposure level (PEL) of formaldehyde as 0.75 ppm calculated for an 8 h time-weighted-average (TWA) for all workers, while short-term exposure level (STEL) as 2 ppm calculated for a 15 min TWA.[5]

In the past, several carcinogenicity and cytogenetic studies have firmly established formaldehyde as a toxic substance that can cause redundant diseases such as irritation of sensory organs, e.g. skin, eyes, throat, and nose, respiratory sensitization as well as acute and chronic diseases, e.g. nasal tumours and cancers.[1,6–9] It is therefore important to monitor the indoor airborne concentration of formaldehyde, which demands the production of inexpensive, small, and portable, yet highly sensitive and selective sensing devices. To date colorimetric devices have shown great promise in direct detection of gaseous formaldehyde.[10–12] These devices are based on a sensitive surface doped with a sorbent, which changes colour on reaction with formaldehyde, and exhibit good selectivity and miniaturization capacity.[13] However, irreversibility and accurate real-time measurements still remain a challenge for these colorimetric formaldehyde assays.[14]

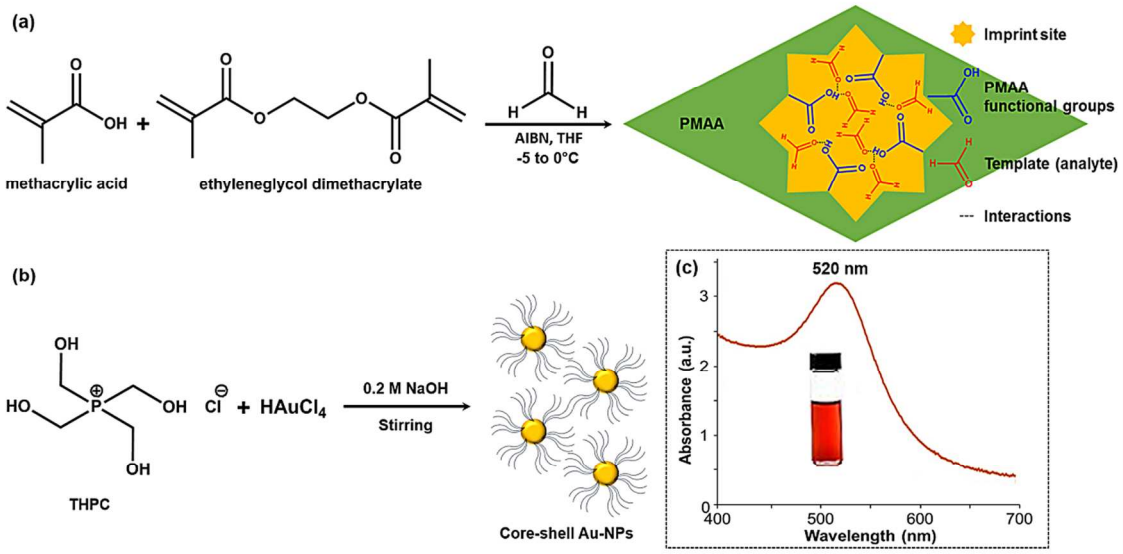

Figure 1. A schematic representation of (a) low-temperature synthesis of formaldehyde imprinted poly(methacrylic acid) – (imp-PMAA), and (b) synthesis of core-shell gold nanoparticles (Au-NPs). (c) UV-vis absorption spectrum of synthesized Au-NPs suspension in water showing absorption at 520 nm.

Conversely, oxide based resistive devices for gaseous formaldehyde detection suffer from high temperature operation requirement and moisture interference.[15–18] It is therefore anticipated that novel fast-responding, selective materials are designed for room temperature recognition and quantification of formaldehyde gas. In this context, pristine polymers and polymer based nanocomposites have emerged as promising alternatives for room temperature formaldehyde detection.[19–21] For instance, graphene/ poly(methyl methacrylate) nanocomposites have recently been reported to exhibit highly selective response to formaldehyde and very low detection limit (10 ppb). However, this nanocomposite system has shown poor reversibility and slow response time (i.e. >10 min), which render its practical applications in indoor air quality control.

Herein, we report a novel strategy based on layer-by-layer assembly of low-temperature formaldehyde imprinted poly(methacrylic acid) (imp-PMAA) and gold nanoparticles (Au-NPs) to fabricate sensitive and selective imp-PMAA/Au-NPs hybrid coatings for quartz microbalance (QMB) transducers. PMAA is a material of choice for preparing formaldehyde imprinted matrix due to the possibility of non-covalent interactions between the polymeric carboxylic acid groups and the template, which may induce selectivity and enhance sensor layer's performance. Furthermore, layer-by-layer assembly[22,23] approach is employed in this study to allow the fabrication of imp-PMAA/Au-NPs sandwich or hybrid layer with orderly structure and optimized thickness. The acidic moieties in imp-PMAA are also expected to interact with Au-NPs leading to the formation of a stronger interface and controlled architecture.[24] Consequently, QMB devices coated with imp-PMAA/Au-NPs hybrid exhibit remarkable form-aldehyde sensor characteristics at room temperature, which make them potentially useful for real-world applications.

Experimental

Materials

The chemicals utilized in this study were of highest available purity and were used without further purification unless stated otherwise. The monomers methacrylic acid (MAA; 99%, with 250 ppm of MEHQ inhibitor) and ethylene glycol dimethacrylate (EGDMA; 98%, with 90-110 ppm of MEHQ inhibitor), the initiator 2,2'-azobisisobutyronitrile (AIBN; 20 wt. % in acetone), paraformaldehyde (PFA; reagent grade, crystalline) for production of the template - formaldehyde (H_2CO), sodium hydroxide (NaOH; ≥98%, anhydrous), hydrogen tetrachloroauric acid ($HAuCl_4$; 99.99% trace metal basis; 30 wt. % in dilute HCl), tetrakis(hydroxymethyl) phosphonium chloride (THPC; 80% in H_2O), and the organic solvents methanol (≥99.8%, anhydrous), acetone (≥99.9%), tetrahydrofuran (THF; ≥99.9%, anhydrous) were obtained from Sigma-Aldrich. AIBN was purified by recrystallization in methanol at -5 to 0°C before use. The inhibitor, monomethyl ether of hydroquinone (MEHQ), was removed from the monomer and crosslinker by washing 3-4 times with 10% NaOH solution prior to use.

Synthesis of molecularly imprinted poly(methacrylic acid)

Formaldehyde imprinted poly(methacrylic acid) pre-polymer (imp-PMAA) was prepared at low temperature (–5 to 0°C) to facilitate complex formation between monomers and template.[25,26] **Figure 1a** exhibits the schematic representation of the procedure for synthesis of formaldehyde imprinted pre-polymer (imp-PMAA). Precisely,

138 µL of methacrylic acid (MAA; the functional monomer), 168 µL of ethylene glycol dimethacrylate (EGDMA; the crosslinker), and 1-2 mg of AIBN (the initiator) were first dissolved in 664 µL of THF in a test tube wrapped in Al foil. The stirring solution was kept in dark at -5 to 0°C. Formaldehyde (the template) vapours were produced by gentle heating of ~5 g of paraformaldehyde in a test tube and dissolved in the monomer solution at -5 to 0°C using a U-shaped glass tube and cork head. After the reaction mixture was flooded with formaldehyde vapours for 10-15 min, the polymerization was initiated under UV light at 0°C. UV 250 W curing hand lamp with 315-405 nm wavelength was used to irradiate the reaction mixture from a distance of 20 cm for 45-60 min to polymerize the reactants. Afterwards, the pre-polymer was stored at -4°C before fabrication of sensing layers. 2-3 µL of the formaldehyde imp-PMAA pre-polymer were spin coated on QMB devices and thermally treated at 60°C for 1 h to remove the template, solvent molecules, and to crosslink polymer. The existence of non-covalent interactions such as hydrogen bonds between the template and the carboxylic acid groups leads to the formation of imprinted PMAA.[19] Thanks to their reversible interactions with the polymeric matrix, formaldehyde molecules can be removed from the polymer bulk by mild heating or washing with a polar solvent after the fabrication of sensitive layers, thus leaving behind molecular cavities (or imprints), as shown in **Figure 1a.**

Synthesis of core-shell gold nanoparticles

Figure 1b demonstrates synthesis of core-shell gold nanoparticles (Au-NPs). Au-NPs were synthesized via slightly modified Duff procedure,[27,28] as reported earlier.[29] In brief, a colloidal suspension of core-shell Au-NPs was prepared by mixing 1 mL of 0.2 M aqueous NaOH, 1 mL of aqueous THPC solution prepared by diluting 0.8 mL of 80% THPC to 100 mL with deionized water, and 1 mL of 0.1 M aqueous $HAuCl_4$ in 37 mL deionized water under continuous stirring. Colloidal core-shell Au-NPs of approximately 10-12 nm diameter were synthesized as a result, exhibiting a sharp plasmon absorption band at 520 nm wavelength (the respective UV-vis spectrum is shown in **Figure 1c**).[28,30] Later, 2-3 µL of colloidal gold suspension were spin coated on bare Au electrode or those pre-coated with imp-PMAA, and thermally treated at 200°C for 2 h.

Fabrication of QMB devices: Layer-by-layer assembly of imp-PMAA/Au-NPs hybrid

A schematic representation of the layer-by-layer assembly of imp-PMAA and Au-NPs to form a sandwich or hybrid sensing layer on the surface of QMB working electrode is shown in **Figure 2a**. Imp-PMAA/Au-NPs hybrid or sandwich structures were fabricated on 10 MHz QMB devices via layer-by-layer assembly and thermal treatment. For this purpose, 2-3 µL of (a) imp-PMAA pre-polymer, (b) core-shell Au-NPs, and (c) imp-PMAA pre-polymer (again) were spin coated on the surface of a QMB electrode at room temperature with a spin speed of 1000 rpm. After coating each layer, the devices were thermally annealed at moderately high temperatures, i.e. 60° or 200°C, for 1-2 h to crosslink PMAA pre-polymer and to remove template and solvent molecules, as well as to partially anneal Au-NPs. In this way, Imp-PMAA is believed to yield a spatially stable organic structure that sandwiches gold nanoparticles by forming coordination linkages between the carboxylic acid groups of imp-PMAA and Au-NPs.[24,31]

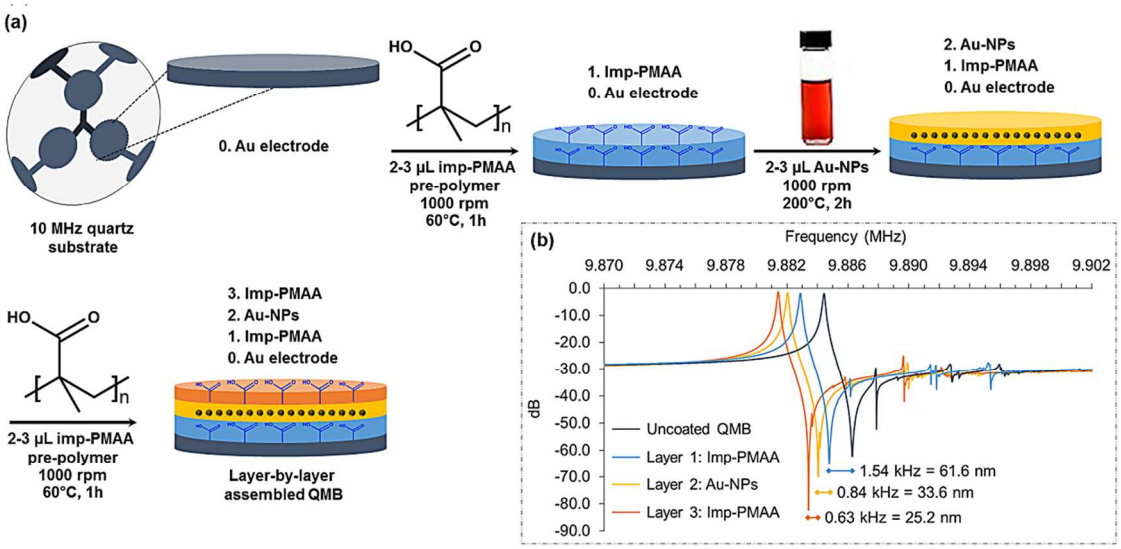

Figure 2. (a) Layer-by-layer assembly of formaldehyde imprinted pre-polymer (imp-PMAA) and colloidal gold nanoparticles (Au-NPs) on 10 MHz QMB for fabrication of imp-PMAA/Au-NPs hybrid or sandwich structures. (b) The frequency and damping characteristics of imp-PMAA/Au-NPs hybrid sensor during the step-wise fabrication or layer-by-layer assembly process. Layer thickness is calculated from the frequency difference (Δf) as a result of mass deposition and is optimized as 100±20 nm corresponding to Δf = 2.5±0.5 kHz.

The step-wise process of layer-by-layer assembly and fabrication of imp-PMAA/Au-NPs hybrid on QMB electrode is monitored by studying the frequency and damping characteristics of QMB with the help of an Agilent E5072A ENA Series network analyser. **Figure 2b** shows the frequency and damping characteristics of QMB before coating and after fabrication and thermal treatment of each layer. Thickness of the imp-PMAA/Au-NPs hybrid layer is calculated by the loss in frequency, i.e. 1 kHz frequency loss corresponds to 40 nm average layer thickness.[32,33] Thus, average thickness of the layers is tailored around 100 ± 20 nm (2-3 kHz) by controlling the amount of material spin-coated at 1000 rpm during the layer-by-layer deposition procedure.

Characterization

The surface morphology of different sensing layers was studied by scanning electron microscopy: model. ∑igma Zeiss. The sensing layers were examined by in-lens detector at 10-20 keV. SEM images are further processed and analysed with the help of Java image processing and analysis program – ImageJ.

Sensor Measurements

Dual or tri-electrode 10 MHz quartz microbalances (QMBs) were used as transducers in sensor fabrication. The measuring electronic and mechanical modules were the same as used in previous studies.[29,34] For control measurements, two tri-electrode QMB devices were mounted in parallel in the sensing chamber. A variety of sensing materials were fabricated on these tri-electrode QMB devices by spin coating 2-5 µL of (a) non-imp-PMAA, (b) imp-PMAA, (c) core-shell Au-NPs, (d) layer-by-layer assembled non-imp-PMAA/Au-NPs hybrid, and (e) layer-by-layer assembled imp-PMAA/Au-NPs hybrid at 1000 rpm spin speed, while a bare Au electrode served as the reference. On the other hand, to determine the formaldehyde sensing characteristics of imp-PMAA/Au-NPs hybrid sensor, a dual-electrode QMB device (with a bare Au reference electrode and a working electrode) was fabricated via layer-by-layer assembly of imp-PMAA and Au-NPs, as discussed above. All sensing experiments were performed at room temperature (25°C) and 50% RH, unless otherwise stated.

Results and Discussion

Characterization

Figure 3 shows the scanning electron micrograph and 2D (2-dimensional) colour intensity map along with surface profile of the formaldehyde imprinted PMAA (imp-PMAA). The SEM image exhibits homogeneous surface morphology with several interconnected nanoscale cracks on the surface. The depth of these cracks is measured as 40-80 nm, while average imp-PMAA layer thickness is around 100 nm (2.5 kHz). Since a dilute imp-PMAA pre-polymer solution is used to fabricate thin sensing layers, these cracks could be formed by the evaporation of excess solvent as well as template molecules during thermal treatment of imp-PMAA layer at 60°C for 1 h. **Figure S1** (see Electronic Supplementary Information (ESI)) shows 3D surface plot constructed from the original SEM image, which further complements the surface topography of imp-PMAA sample.

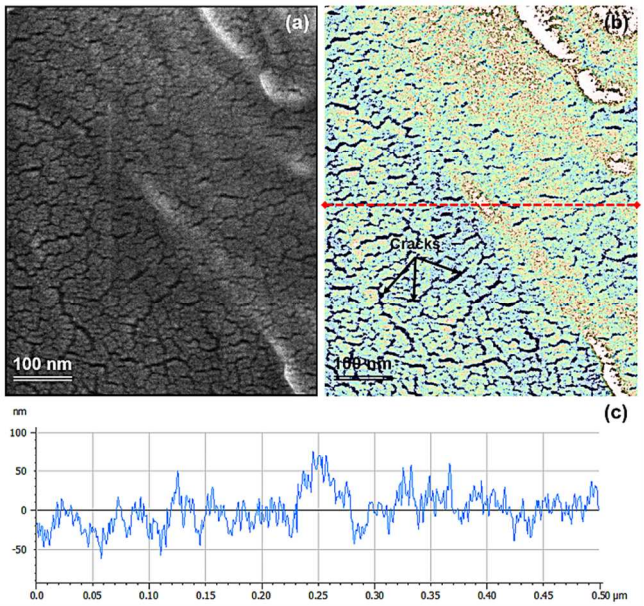

Figure 3. (a) Scanning electron micrograph, (b) corresponding 2D colour intensity map, and (c) surface profile of formaldehyde imprinted PMAA (imp-PMAA) layer after spin coating and thermal annealing at 60°C for 1 h.

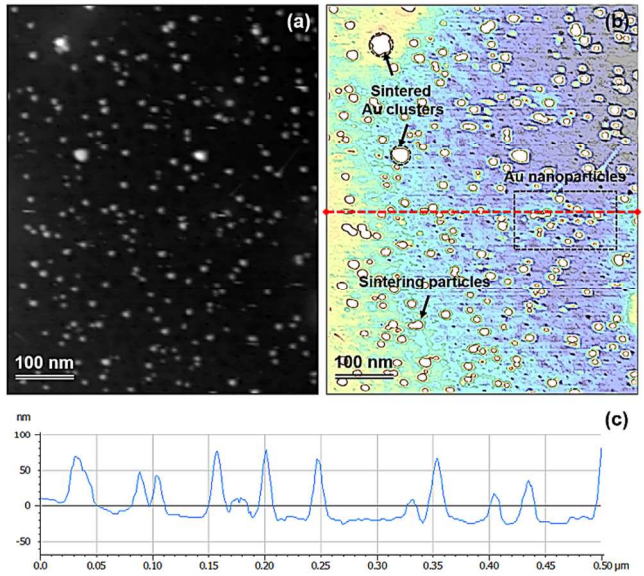

Figure 4. (a) Scanning electron micrograph, (b) corresponding 2D colour intensity map, and (c) surface profile of core-shell gold nanoparticles (Au-NPs) after spin coating and thermal annealing at 200°C for 2 h.

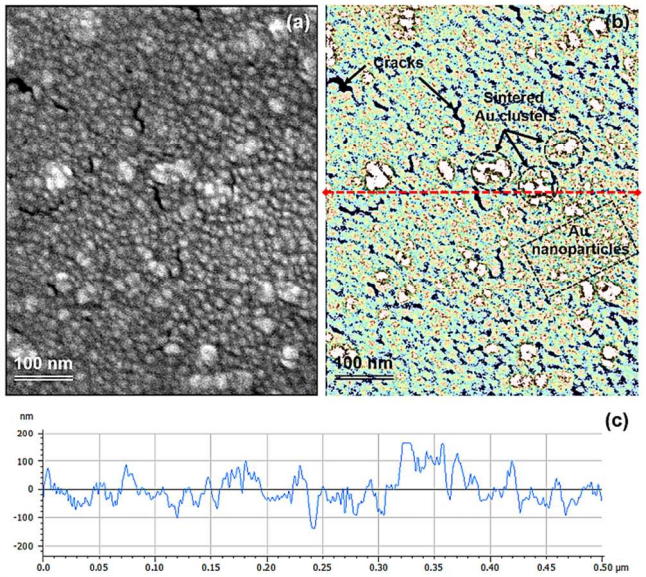

Figure 5. (a) Scanning electron micrograph, (b) corresponding 2D colour intensity map, and (c) surface profile of layer-by-layer assembled imp-PMAA/Au-NPs hybrid. The assembly process and layer sequence is shown in Figure 2a.

Au-NPs layer, on the other hand, exhibits scattered distribution of Au-NPs on the surface of electrode, as shown in **Figure 4**. In addition, **Figure S2** (see ESI) presents 3D surface plot of an Au-NPs layer showing several protrusions on the surface, which can be recognised as Au nanoparticles and clusters depending on their sizes. The size of individual Au-NPs is in the range of 8-14 nm. Certain bigger particles or clusters formed by sintering of two or more Au-NPs are also observed. The size of these Au clusters varies between 25-35 nm. The coalescence of Au-NPs is also expected as a result of thermal annealing at 200°C for 2 h;[35] however, majority of Au-NPs retain their size and shape due to scattered arrangement of Au-NPs. The average thickness of Au-NPs layer is measured as ~84 nm (2.1 kHz).

Scanning electron micrograph of layer-by-layer assembled imp-PMAA/Au-NPs hybrid is shown in **Figure 5** along with 2D colour intensity map and surface profile. The image shows the characteristics of imp-PMAA as well as Au-NPs layers. The presence of individual Au-NPs nanoparticles and some nanoparticulate clusters embedded into imp-PMAA matrix is observed along with some cracks on the surface. Thickness of the imp-PMAA/Au-NPs hybrid layer is measured to be 121 nm (~3.0 kHz). The number of cracks on the hybrid surface is significantly reduced by layer-by-layer assembly of imp-PMAA and Au-NPs and resulting interlayer chemical interactions.[24,31] 3D surface plot of the imp-PMAA/Au-NPs hybrid layer also confirms these observations, as shown in **Figure S3** (see ESI). The image also displays homogeneous surface topography and roughness. Furthermore, the distribution of nanoparticles in hybrid layer is found to be uniform instead of scattered dispersion shown by pristine Au-NPs layer due to better anchoring of Au-NPs on the polymer surface as compared to bare Au electrode.

Control Measurements: Detection of Formaldehyde

In this study, two parallel tri-electrode QMBs are used with one uncoated (or reference) electrode and five working electrodes coated with different sensing materials: (a) non-imp-PMAA, (b) imp-PMAA, (c) pristine or colloidal Au-NPs, (d) non-imp-PMAA/Au-NPs hybrid, and (e) imp-PMAA/Au-NPs hybrid. The sensing layers are fabricated by spin coating, and the devices are thermally annealed at 60-200°C before mounting them in the sensing chamber for gaseous formaldehyde detection. As stated earlier, thickness of the layers is measured and optimized as 100 ± 20 nm. Furthermore, the sensor response (Δf) of each layer is normalized to Hz per 1 kHz (~40 nm) of layer thickness in order to offer real-time comparison of the sensitivity of different materials.

Figure 6 shows the normalized sensor response of QMB devices coated with different sensing materials toward 1 ppm formaldehyde vapours in air at 25°C and 50% relative humidity (RH). Imp-PMAA/Au-NPs hybrid evidently produces the highest sensor effect for 1 ppm formaldehyde compared to other sensitive layers. The normalized sensor response of different sensing materials in decreasing order is: imp-PMAA/Au-NPs (7.9 Hz kHz^{-1}) > Au-NPs (5.4 Hz kHz^{-1}) > imp-PMAA (4.8 Hz kHz^{-1}) > non-imp-PMAA/Au-NPs (0.9 Hz kHz^{-1}) > non-imp-PMAA (0.5 Hz kHz^{-1}).

Both pristine Au-NPs and imp-PMAA layers show comparable sensor effect, though based on different sensing mechanism, i.e. different types of interactions. Au-NPs are most likely to exhibit high sensitivity owing to their high surface availability and affinity interactions between the aldehyde oxygen and Au-NPs.[36] On the contrary, imp-PMAA provides imprint sites for shape-specific molecular recognition of formaldehyde and its non-covalent interactions with carboxylic acid groups.[19] Therefore, layer-by-layer assembled imp-PMAA/Au-NPs hybrid structure simultaneously provides both high surface area and imprint sites to formaldehyde molecules leading to 1.5-8.6 fold increase in sensor effect. After the control measurements are performed, imp-PMAA/Au-NPs hybrid is selected for further experiments due to its higher sensitivity toward gaseous formaldehyde.

Formaldehyde Sensing Characteristics of Imp-PMAA/ Au-NPs Hybrid

To further investigate the sensing properties of layer-by-layer assembled imp-PMAA/Au-NPs hybrids, dual electrode QMB devices are fabricated and mounted in the sensing chamber. The working electrode of QMB device is coated with imp-PMAA/Au-NPs hybrid layer, while an uncoated (Au) electrode is set as reference. To estimate the selectivity of imp-PMAA/Au-NPs hybrid, the devices are exposed to different concentrations of formaldehyde and interfering analytes at room temperature and 50% RH.

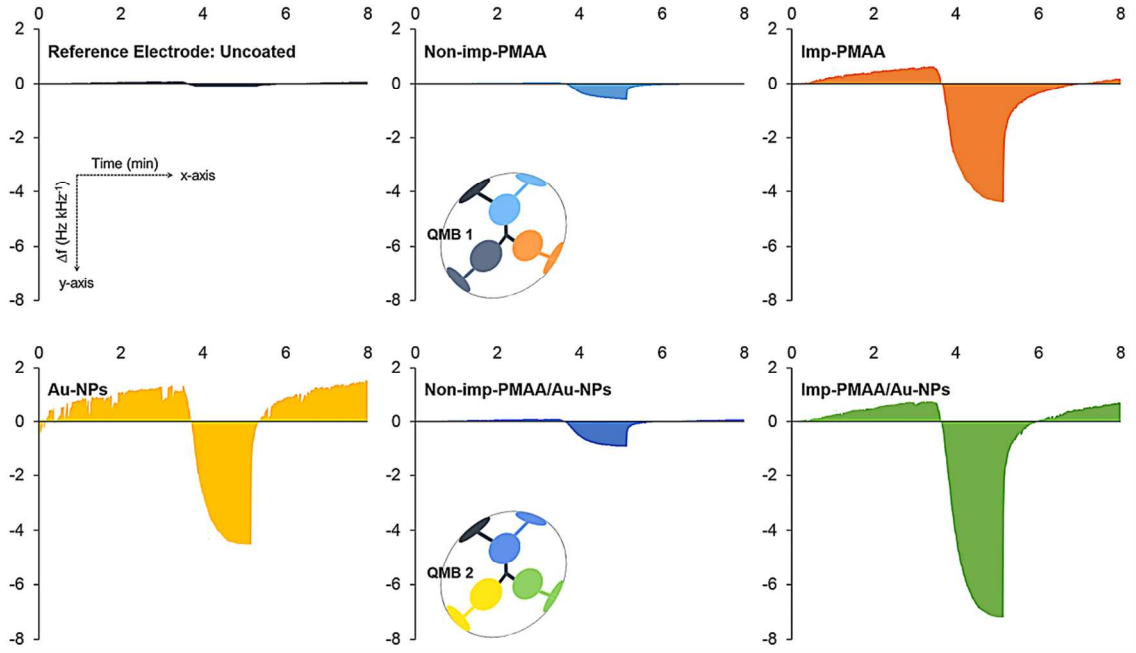

Figure 6. Control experiments: Time-dependent frequency response of two tri-electrode QMB devices coated with different sensing materials toward 1 ppm formaldehyde gas at 25°C and 50% RH. These sensor responses are normalized to 1 kHz or 40 nm of layer thickness.

Figure 7 shows the normalized sensor response of imp-PMAA/Au-NPs hybrid to formaldehyde and interfering gases such as acetone, methanol, and water vapours. Acetone is selected as an interferent due to presence of carbonyl moiety that may interact with and block the imprint sites, while methanol is preferred because of possible hydrogen bond interactions with PMAA. Water (% RH), however, is one of the most common interfering substance during real-time sensing of indoor air quality.[17,37] In addition to possible hydrogen bonding interactions with PMAA, water vapours are reported to have a detrimental effect on formaldehyde sensors' performance.[38,39]

Thus, considering the specific interactions such as hydrogen bonding or weaker dipole-dipole forces between the interfering gases and the imp-PMAA/Au-NPs hybrid material, the sensor exhibits very selective response toward formaldehyde that may be attributed to the imprinting effect of formaldehyde.[40] At low concentration (10-20 ppm) of analyte gases, the sensor effect of imp-PMAA/Au-NPs hybrid layer toward formaldehyde is 3-4 fold higher than those of methanol and acetone, while 6-8 times that of 10-20% RH. The results suggest that neither acetone (based on affinity interactions) nor methanol and water (based on possible hydrogen bonding) cause frequency shift comparable to formaldehyde (based on template specific interactions at imprint sites). These observations are consistent with the molecular recognition phenomenon, as already established by previous reports.[41–46]

According to these reports,[41-46] the selectivity pattern of an imprinted material is primarily determined by the nature of polymer, template, and interactions between them as well as polymerization conditions. Under optimal conditions, non-covalent imprinting leads to the formation of molecular cavities that are chemical and geometrical fit for the template molecules. Thus, size- and shape-tailored molecular cavities or imprints, as shown in Figure 1a, act as pre-organized binding sites for the target analyte, e.g. formaldehyde in this case. This leads to improved selectivity of the vapour sensor.

Table 1. Sensor response characteristics of layer-by-layer assembled imp-PMAA/Au-NPs hybrid toward different gases.

Analyte Gas	Molecular weight (g mol^{-1})	Boiling point (°C)	Sensor effect[a,b] (Hz kHz^{-1})	Sensor characteristics from calibration curve			Linear response range
				Slope [c]	Intercept	R^2	
Formaldehyde (ppm)	30.03	-19.0	-21.8	0.295	-7.47	0.99	1-50
Acetone (ppm)	58.08	56.0	-11.4	0.080[d]	-4.11	0.96[d]	20-50
Methanol (ppm)	32.04	64.7	-10.1	0.156	-3.05	0.97	10-50
RH (%)	18.01	100.0	-3.2	0.020[d]	-1.88	0.99[d]	20-50

[(a)] Sensor effect is normalized to 1 kHz (~40 nm) layer thickness and is corrected, i.e. sensor effect of reference Au electrode is subtracted; [(b)] Herein, sensor effects are reported for 50 ppm organic gas concentration and 50% relative humidity (RH); [(c)] Slope represents sensitivity of imp-PMAA/Au-NPs hybrid layer in Hz kHz^{-1} ppm^{-1}; [(d)] In case of near-saturation sensor response, slope and R^2 values are calculated over a linear response range of 20-50 ppm acetone and 20-50 % RH.

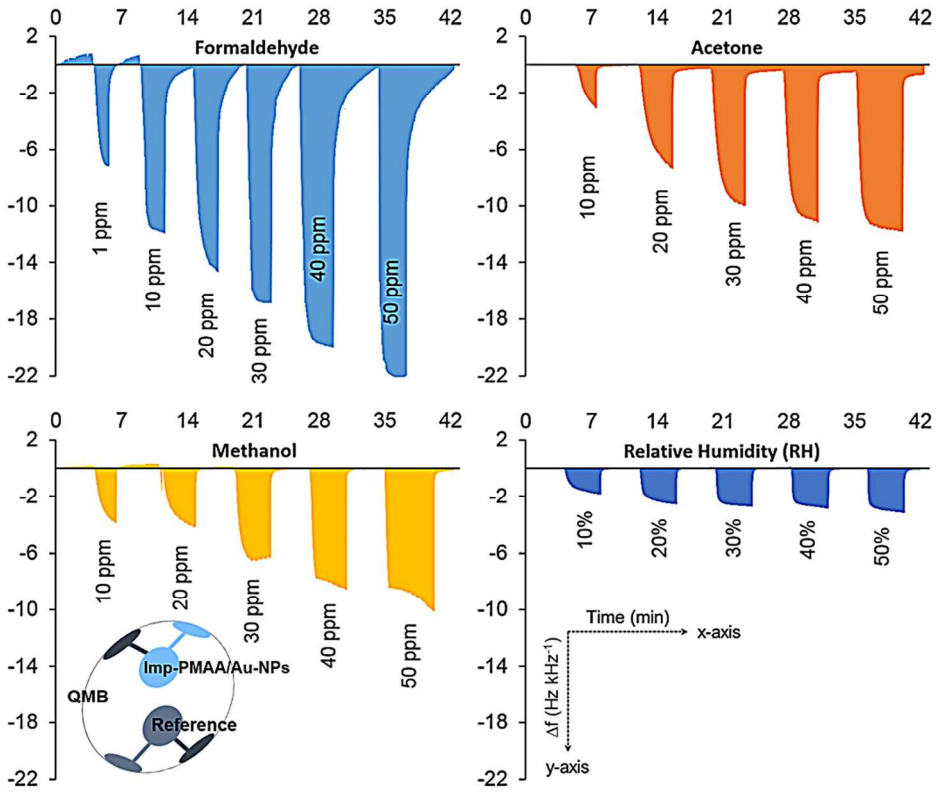

Figure 7. The time dependent frequency response of dual-electrode 10 MHz QMB sensor coated with layer-by-layer assembled imp-PMAA/Au-NPs hybrid toward different concentrations of formaldehyde and interfering gases: acetone, methanol, and water (% RH) at 25°C. The sensor responses are normalized to 1 kHz or 40 nm of layer thickness and corrected by subtracting the frequency response of reference (uncoated) electrode.

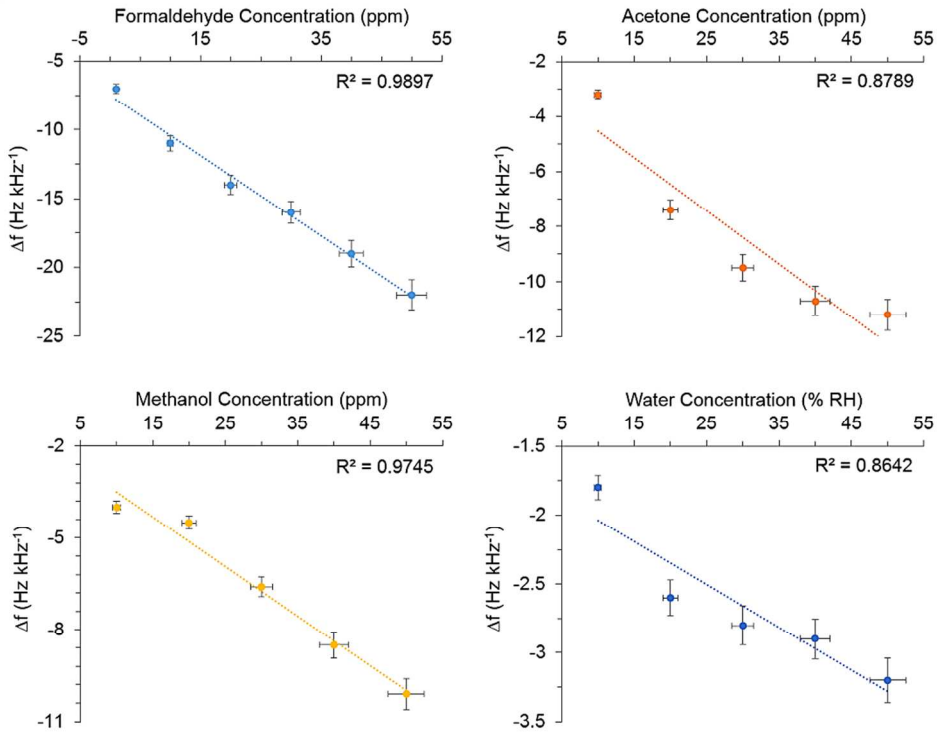

Figure 8. The calibration curves: Normalized and corrected frequency shift of dual-electrode 10 MHz QMB sensor coated with imp-PMAA/Au-NPs hybrid layer is drawn against different concentrations of gaseous analytes: formaldehyde, acetone, methanol, and water (% RH).

Figure 8 shows the comparison of imp-PMAA/Au-NPs hybrid sensor's effect toward formaldehyde, acetone, methanol, and RH (%) at different gaseous analyte concentrations. The sensor demonstrates linear response toward formaldehyde and methanol, while non-linear or near-saturation response toward acetone and RH. The data obtained from these calibration curves are recorded in **Table 1** along with physical properties of the analyte gases to further study the selectivity pattern of hybrid layer. The slope of calibration curve roughly estimates the sensitivity of sensing material toward different gases.[29] It shows that imp-PMAA/Au-NPs hybrid sensor exhibits approximately two-fold higher sensitivity (in Hz kHz^{-1} ppm^{-1}) toward formaldehyde as compared to that of methanol, which is second in the list. The insignificant interference signals of acetone and water vapours (% RH), on the other hand, may only arise from weak physical/non-specific dispersion interactions.[47]

To test the short-term reproducibility and repeatability of imp-PMAA/Au-NPs hybrid sensor, it is exposed to multiple pulses of 1 ppm formaldehyde gas at room temperature and 50% RH. **Figure 9a** shows the time-dependent frequency response of the hybrid sensor indicating excellent reproducibility of the sensor signal with 7.266 ± 0.015 Hz kHz^{-1} sensor effect. Thus, QMB sensors coated with imp-PMAA/Au-NPs hybrid are very stable and exhibit reliable performance at low concentration of formaldehyde. The response of hybrid layer toward formaldehyde is completely reversible, as shown in **Figure 9a**, and no hysteresis is seen during the measurements. **Figure 9b** demonstrates typical response (T_{res90}) and recovery (T_{rec90}) times of the same device working under 1 ppm formaldehyde at room temperature and 50% RH. It is observed that 90% of the total frequency shift takes place within 28 ± 5 sec, and 90% of the corresponding sensor signal is recovered within 13 ± 5 sec indicating fast response and recovery kinetics of imp-PMAA/Au-NPs hybrid sensor.

Furthermore, threshold limit of detection (LoD) can be calculated from the repeatable measurements using linear regression method,[29] which is given by: LoD = 3σ/S, where S is the sensitivity of the hybrid layer (sensor) estimated from the calibration curve, and σ is the standard deviation of the sensor response at 1 ppm formaldehyde. Thus calculated LoD for imp-PMAA/Au-NPs hybrid sensor is 152.5 ppb, which is well below the PEL of formaldehyde 750 ppb set by OSHA for 8 h TWA.[5] On the basis of these results, it can be established that layer-by-layer assembled imp-PMAA/Au-NPs hybrid structure is an excellent candidate for improving the performance of QMB formaldehyde sensors. A comparison of the performance parameters of recently reported formaldehyde sensors with this work is presented in **Table 2**, which clearly indicates the superior overall performance of the imp-PMAA/Au-NPs hybrid sensor toward formaldehyde gas.

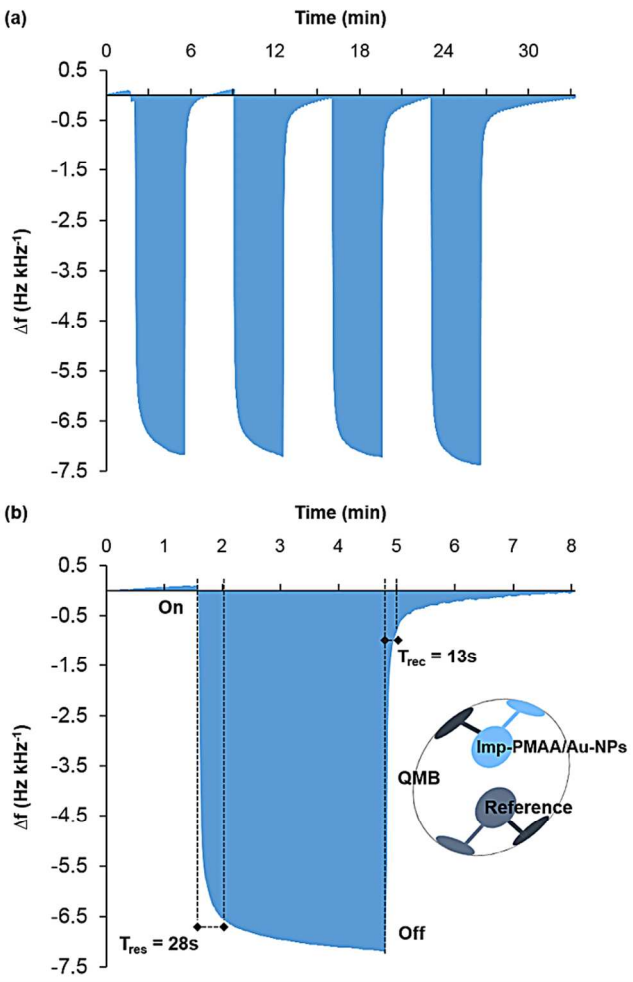

Figure 9. (a) Short-term reproducibility, and (b) response-recovery kinetics of a dual-electrode 10 MHz QMB sensor coated with layer-by-layer assembled imp-PMAA/Au-NPs hybrid toward 1 ppm formaldehyde at 25°C and 50% RH.

In summary, we believe that enhanced sensor performance of the new layer-by-layer assembled imp-PMAA/Au-NPs hybrid material is principally governed by the following factors: First, low-temperature formaldehyde imprinting of PMAA pre-polymer leads to the formation of size and shape specific interaction sites within the pre-polymer for selective detection of formaldehyde;[48,25] second, the presence of nanoscale gold particles sandwiched between PMAA increases the surface-to-volume ratio and sensitivity of the fabricated layer and produces new material with synergistic sensing properties;[49,50] and most importantly third, the layer-by-layer assembly of imp-PMAA and Au-NPs offers greater precision in the formation of hybrid or sandwich architecture with controlled thickness,[22,50] thus leading to the structural stability and excellent reproducibility of the sensor effect.

Table 2. A comparison of the layer-by-layer assembled imp-PMAA/Au-NPs hybrid sensor's performance with recently reported formaldehyde detection systems.

Sensing material	Transduction principle	Operating temperature (°C)	Limit of detection (ppb)	Response kinetics (sec)		Linear response range (ppm)	Selectivity/ Humidity effect	Reference
				T_{res90}	T_{rec90}			
Imp-PMAA/Au-NPs hybrid	QMB-gravimetric	25	152.5	28	13	1-50	Good/ Negligible	This work
Amino-SBA-15 [a]	QMB-gravimetric	25	≤500	11	15	0.5-50	Good/-	Zhu et al.[47]
Graphene/PMMA	Chemiresistor	25	10	≥600	~100	0.05-5	Good/-	Alizadeh et al.[20]
PANi/PEI composite [b]	Chemiresistor	25	ppm [e]	≥400	-	37.7-189	Good/-	Antwi-Boampong et al.[21]
TFQ@SWCNTs [c]	Chemiresistor	-	≤150	≥60	~60	0.15-1.2	Good/ Problematic	Shi et al.[38]
Pd-SnO_2 nanofibers	Chemiresistor	190	50	53	103	0.05-0.5	Good/-	Tian et al.[51]
Co-doped SnO_2 microcubes	Chemiresistor	260	sub-ppm [e]	4	18	25-400	Sufficient/-	Huang et al.[52]
Core-shell Au@SnO_2	Chemiresistor	25-55	sub-ppm [e]	80	62	20-50	Good/ Problematic	Chung et al.[39]
P3HT/Fe_2O_3 composite [d]	OTFT-transistor	25	ppm [e]	≥60	≥600	100	-	Tai et al.[53]
Ag/Y-codoped $LiFe_{1-0.01x}PO_4$	Optical waveguide	-	1	~20	≥300	0.1-100	Good/-	Nizamidin et al.[54]

[a] Amine-functionalized SBA-15; [b] Poly(aniline)/poly(ethyleneimine) composite; [c] Tetrafluorohydroquinone functionalized single-walled carbon nanotubes; [d] Poly(3-hexylthiophene)/ferric oxide nanocomposites; [e] Detection limits are roughly estimated from the data presented in the reference.

Conclusions

A facile and effectively reproducible layer-by-layer assembly method is reported for the fabrication of formaldehyde imprinted PMAA and Au-NPs hybrid or sandwich structures on 10 MHz QMB devices. The hybrid structure is studied by SEM indicating Au-NPs homogeneously distributed into the polymer sandwich. The QMB devices coated with imp-PMAA/Au-NPs hybrid layer are subsequently exposed to different analyte gases including formaldehyde, acetone, methanol, and water vapours (% RH). The sensor exhibits: (a) High sensitivity toward gaseous formaldehyde; (b) low cross-sensitivity toward interfering gases and humidity; (c) fast response and recovery time; (d) complete reversibility and good short-term repeatability; and (e) very low threshold detection limit; (f) at room temperature. We conclude that low-temperature formaldehyde imprinting combined possibly with greater surface area of Au-NPs in an imp-PMAA/Au-NPs hybrid layer ensures high sensitivity and selectivity toward formaldehyde and indicates that layer-by-layer assembled hybrid sensors may be considered as excellent candidates for gaseous formaldehyde sensing applications.

Acknowledgements

Authors thank Professors F. L. Dickert and P. A. Lieberzeit (University of Vienna, Austria) for their profound support and continuous guidance in research and discussion, and Professors L. Torsi and N. Cioffi (University of Bari, Italy) for their assistance.

Notes and references

[a] Institute of Analytical Chemistry, University of Vienna, Waehringer-strasse 38, A-1090, Vienna, Austria.
[b] Department of Chemistry, University of Bari, via Orabona 4, 70126, Bari, Italy.
[c] Present Address: Department of Biosciences, COMSATS Institute of Information Technology, Chak Shahzad, 45600, Islamabad, Pakistan.
[d] Present Address: Affiliated Colleges at Hafr Al-Batin, King Fahd University of Petroleum and Minerals, P.O. Box 1803, 31991, Hafr Al-Batin, Saudi Arabia. Phone: +966 (0) 13 720 3426 ext. 1675; Email: aa@aafzal.com
[e] Present Address: Institute of Chemistry, University of Punjab, Quaid-e-Azam Campus, 54590, Lahore, Pakistan.

† Electronic Supplementary Information (ESI) available: 3D surface plots of imp-PMAA, Au-NPs, and imp-PMAA/Au-NPs hybrid layers.

1. IARC Working Group on the Evaluation of Carcinogenic Risks to Humans, Ed., *A review of human carcinogens*, International Agency for Research on Cancer, World Health Organization, Lyon, 2012, vol. 100F.
2. J. D. McDonald, B. Zielinska, E. M. Fujita, J. C. Sagebiel, J. C. Chow, and J. G. Watson, *Environ. Sci. Technol.*, 2000, **34**, 2080–2091.
3. H. Guo, S. C. Lee, L. Y. Chan, and W. M. Li, *Environ. Res.*, 2004, **94**, 57–66.
4. T. Salthammer, S. Mentese, and R. Marutzky, *Chem. Rev.*, 2010, **110**, 2536–2572.
5. *OSHA Factsheet: Formaldehyde*, Occupational Safety and Health Administration, 2011.
6. O. Demkiv, O. Smutok, S. Paryzhak, G. Gayda, Y. Sultanov, D. Guschin, H. Shkil, W. Schuhmann, and M. Gonchar, *Talanta*, 2008, **76**, 837–846.

7. L. E. B. Freeman, A. Blair, J. H. Lubin, P. A. Stewart, R. B. Hayes, R. N. Hoover, and M. Hauptmann, *J. Natl. Cancer Inst.*, 2009, **101**, 751–761.
8. P. Wolkoff and G. D. Nielsen, *Environ. Int.*, 2010, **36**, 788–799.
9. G. D. Nielsen and P. Wolkoff, *Arch. Toxicol.*, 2010, **84**, 423–446.
10. L. Feng, C. J. Musto, and K. S. Suslick, *J. Am. Chem. Soc.*, 2010, **132**, 4046–4047.
11. X. Wang, Y. Si, J. Wang, B. Ding, J. Yu, and S. S. Al-Deyab, *Sens. Actuators B Chem.*, 2012, **163**, 186–193.
12. X. Wang, Y. Si, X. Mao, Y. Li, J. Yu, H. Wang, and B. Ding, *Analyst*, 2013, **138**, 5129–5136.
13. K. Kawamura, K. Kerman, M. Fujihara, N. Nagatani, T. Hashiba, and E. Tamiya, *Sens. Actuators B Chem.*, 2005, **105**, 495–501.
14. A. Allouch, M. Guglielmino, P. Bernhardt, C. A. Serra, and S. Le Calvé, *Sens. Actuators B Chem.*, 2013, **181**, 551–558.
15. T. Kida, T. Doi, and K. Shimanoe, *Chem. Mater.*, 2010, **22**, 2662–2667.
16. X. Lai, D. Wang, N. Han, J. Du, J. Li, C. Xing, Y. Chen, and X. Li, *Chem. Mater.*, 2010, **22**, 3033–3042.
17. N. Han, X. Wu, D. Zhang, G. Shen, H. Liu, and Y. Chen, *Sens. Actuators B Chem.*, 2011, **152**, 324–329.
18. A. Afzal, N. Cioffi, L. Sabbatini, and L. Torsi, *Sens. Actuators B Chem.*, 2012, **171-172**, 25–42.
19. L. Feng, Y. Liu, X. Zhou, and J. Hu, *J. Colloid Interface Sci.*, 2005, **284**, 378–382.
20. T. Alizadeh and L. H. Soltani, *J. Hazard. Mater.*, 2013, **248–249**, 401–406.
21. S. Antwi-Boampong and J. J. BelBruno, *Sens. Actuators B Chem.*, 2013, **182**, 300–306.
22. H. Xu, M. Schönhoff, and X. Zhang, *Small*, 2012, **8**, 517–523.
23. Y. Li, X. Wang, and J. Sun, *Chem. Soc. Rev.*, 2012, **41**, 5998–6009.
24. A. N. Shipway, E. Katz, and I. Willner, *ChemPhysChem*, 2000, **1**, 18–52.
25. S. A. Piletsky, E. V. Piletska, K. Karim, K. W. Freebairn, C. H. Legge, and A. P. F. Turner, *Macromolecules*, 2002, **35**, 7499–7504.
26. A. Poma, A. Guerreiro, M. J. Whitcombe, E. V. Piletska, A. P. F. Turner, and S. A. Piletsky, *Adv. Funct. Mater.*, 2013, **23**, 2821–2827.
27. D. G. Duff, A. Baiker, and P. P. Edwards, *Langmuir*, 1993, **9**, 2301–2309.
28. D. G. Duff, A. Baiker, and P. P. Edwards, *J. Chem. Soc. Chem. Commun.*, 1993, 96–98.
29. N. Iqbal and A. Afzal, *Sci. Adv. Mater.*, 2013, **5**, 939–946.
30. S. Link and M. A. El-Sayed, *J. Phys. Chem. B*, 1999, **103**, 4212–4217.
31. P. M. Boltovets, S. A. Kravchenko, and B. A. Snopok, *Plasmonics*, 2010, **5**, 395–403.
32. F. L. Dickert, P. A. Lieberzeit, P. Achatz, C. Palfinger, M. Fassnauer, E. Schmid, W. Werther, and G. Horner, *Analyst*, 2004, **129**, 432–437.
33. R. Schirhagl, U. Latif, D. Podlipna, H. Blumenstock, and F. L. Dickert, *Anal. Chem.*, 2012, **84**, 3908–3913.
34. U. Latif, A. Mujahid, A. Afzal, R. Sikorski, P. A. Lieberzeit, and F. L. Dickert, *Anal. Bioanal. Chem.*, 2011, **400**, 2507–2515.
35. N. Cioffi, L. Colaianni, E. Ieva, R. Pilolli, N. Ditaranto, M. D. Angione, S. Cotrone, K. Buchholt, A. L. Spetz, L. Sabbatini, and L. Torsi, *Electrochimica Acta*, 2011, **56**, 3713–3720.
36. G. Peng, U. Tisch, O. Adams, M. Hakim, N. Shehada, Y. Y. Broza, S. Billan, R. Abdah-Bortnyak, A. Kuten, and H. Haick, *Nat. Nanotechnol.*, 2009, **4**, 669–673.
37. Y. Qiu and S. Yang, *Adv. Funct. Mater.*, 2007, **17**, 1345–1352.
38. D. Shi, L. Wei, J. Wang, J. Zhao, C. Chen, D. Xu, H. Geng, and Y. Zhang, *Sens. Actuators B Chem.*, 2013, **177**, 370–375.
39. F.-C. Chung, R.-J. Wu, and F.-C. Cheng, *Sens. Actuators B Chem.*, 2014, **190**, 1–7.
40. Y. Fu and H. O. Finklea, *Anal. Chem.*, 2003, **75**, 5387–5393.
41. F. L. Dickert and O. Hayden, *Fresenius J. Anal. Chem.*, 1999, **364**, 506–511.
42. L. Ye and K. Mosbach, *Chem. Mater.*, 2008, **20**, 859–868.
43. S. Li, Y. Ge, S. A. Piletsky, and A. P. F. Turner, *Adv. Funct. Mater.*, 2011, **21**, 3344–3349.
44. C. Gonzato, M. Courty, P. Pasetto, and K. Haupt, *Adv. Funct. Mater.*, 2011, **21**, 3947–3953.
45. G. Lautner, J. Kaev, J. Reut, A. Öpik, J. Rappich, V. Syritski, and R. E. Gyurcsányi, *Adv. Funct. Mater.*, 2011, **21**, 591–597.
46. G. Mustafa and P. A. Lieberzeit, *RSC Adv.*, 2014, **4**, 12723–12728.
47. Y. Zhu, H. Li, Q. Zheng, J. Xu, and X. Li, *Langmuir*, 2012, **28**, 7843–7850.
48. C. J. Allender, C. M. Heard, and K. R. Brain, *Chirality*, 1997, **9**, 238–242.
49. G. Decher, *Science*, 1997, **277**, 1232–1237.
50. S. Srivastava and N. A. Kotov, *Acc. Chem. Res.*, 2008, **41**, 1831–1841.
51. S. Tian, X. Ding, D. Zeng, J. Wu, S. Zhang, and C. Xie, *RSC Adv.*, 2013, **3**, 11823–11831.
52. J. Huang, L. Wang, C. Gu, M. Zhai, and J. Liu, *CrystEngComm*, 2013, **15**, 7515–7521.
53. H. Tai, Y. Jiang, C. Duan, W. Dan, and X. Li, *Integr. Ferroelectr.*, 2013, **144**, 15–21.
54. P. Nizamidin, A. Yimit, A. Abdurrahman, and K. Itoh, *Sens. Actuators B Chem.*, 2013, **176**, 460–466.